Available online at www.sciencedirect.com
SCIENCE DIRECT®
Journal of Power Sources 124 (2003) 459–472
JOURNAL OF POWER SOURCES
www.elsevier.com/locate/jpowsour

Development of portable fuel cell arrays with printed-circuit technology

Ryan O'Hayre [a,*], Daniel Braithwaite [b], Weston Hermann [b], Sang-Joon Lee [c], Tibor Fabian [b], Suk-Won Cha [b], Yuji Saito [b], Fritz B. Prinz [a,b]

[a] *Department of Materials Science and Engineering, Rapid Prototyping Laboratory, Stanford University, Room 226, Building 530, Duena St. and Escondido Mall, Stanford, CA 94305-303, USA*
[b] *Department of Mechanical Engineering, Rapid Prototyping Laboratory, Stanford University, Room 226, Building 530, Stanford, CA 94305-303, USA*
[c] *Department of Mechanical & Aerospace Engineering, San Jose State University, San Jose, CA, USA*

Received in revised form 14 June 2003; accepted 14 June 2003

Abstract

Portable hydrogen/oxygen fuel cell power sources were constructed using printed-circuit board (PCB) technology. Multiple iterations of miniature planar fuel cell devices were prototyped, demonstrating fast cycle innovation and dramatic power density improvements in <1 year of development. Several novel flow structure and gas routing designs were explored. Electrical interconnections for configurable voltage were wired on board by printed-circuit traces and vias. Fuel cell device voltages ranging from 1 V single cells to 16 V planar arrays were demonstrated, with power output ranging from <1 to >200 W. The lightweight laminate PCB technology allows the best prototypes to achieve >700 mW/cm^2 area power density and >400 mW/cm^3 volumetric power density. PCB technology offers an intriguing platform for portable fuel cell development below 1 kW. Possibilities for on board diagnostics/control and further power density improvements are envisioned.

Keywords: PEMFC; Miniature; Printed-circuit board; Planar array; Laminate construction; Rapid prototyping

1. Introduction

1.1. PCB and fuel cells

Printed-circuit board technologies (PCB) offer an intriguing platform for portable fuel cell development. Fuel cell prototyping is an unconventional application of PCB technology, requiring a number of non-standard PCB implementations. Nonetheless, PCB technology has been found to be a beneficial platform for portable fuel cell development for several compelling reasons:

- Mature, robust, reliable technology set.
- Fast prototype cycle times.
- Cost efficient prototyping.
- High design flexibility.
- Complex conductor/insulator patterning.
- Low-temperature processing capability.
- Lightweight composite materials.

To our knowledge, we are the first to report the application of PCB technologies to develop fully functional planar array fuel cell devices [1,2]. The use of PCB technologies for miniature fuel cells offers advantages over other design approaches. These include increased design flexibility, potentially higher power densities, ease of device integration, and improved packaging form factors. Making use of the fast prototyping capability of PCB technology, we have been able to fashion at least five iterative generations of PCB fuel cell (PCB-FC) prototypes in under 1 year. This quick turnaround cycle has enabled us to improve device power densities by over two orders of magnitude in that time frame, as well as explore the application of the PCB technology over a range of device sizes. Using a combination of standard and non-standard PCB approaches, we have prototyped a suite of miniature fuel cell devices capable of providing several watts to several hundred watts of power. Several of these PCB-FC devices are pictured in Fig. 1.

1.2. Fuel cell miniaturization

Nearly all modern electronic devices require portable electrical power, and power consumption is often a

* Corresponding author. Tel.: +1-650-725-9936.
E-mail address: rohayre@stanford.edu (R. O'Hayre).

0378-7753/$ – see front matter © 2003 Elsevier B.V. All rights reserved.
doi:10.1016/S0378-7753(03)00802-4

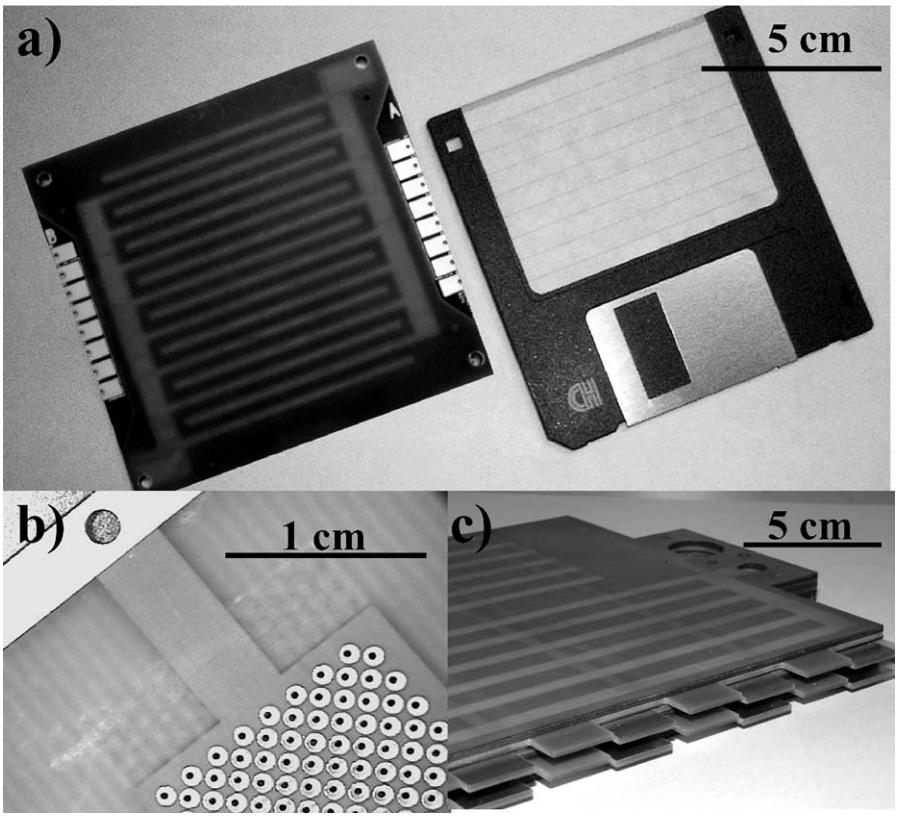

Fig. 1. (a) A 16-cell adhesively laminated PCB-FC device, size compared to a standard 3.5 in. floppy disk. (b) Detail of the PCB inner board for single cell PCB-FC using micro-stitch design. (c) Close up of an adhesively laminated 12-cell double board PCB-FC stack. The dimensions of the three prototypes shown in this figure are given in Table 1.

performance bottleneck. Wireless products, such as personal digital assistants, mobile phones, and next generation laptops in particular have a great demand for sustained power. For long-term, portable operation, fuel cells are an attractive solution. Fuel cells, like batteries, efficiently convert chemical energy into electricity, but have additional advantages, such as higher energy density and the possibility of instant refueling.

In contrast to batteries, unfortunately, fuel cell design is considerably more complicated. A fuel cell device must accomplish several tasks. First, it must be capable of delivering H_2 gas to the anode, and O_2 gas to the cathode (for example, via some type of flow structure). Secondly, these gases must remain isolated from one another; thus sealing is of critical importance. Finally, external electrical access to the anode and cathode electrodes must be provided. This becomes even more important if several fuel cells are to be connected together in series to raise voltage. Electrical interconnection between the cells should be facile, flexible, and low-loss.

To date, the bulk of fuel cell research has focused on large-scale (>1 kW) systems. These systems are intended for use primarily in stationary power applications, where miniaturization is not a concern. In considering fuel cells for portable applications, however, a unique set of design criteria must be applied. This is because the requirements for large-scale fuel cell systems and small-scale fuel cell systems are fundamentally different. The goals of a large-scale fuel cell system are usually maximum efficiency and minimum total cost, while for a small-scale system the goal is maximum power density. Large-scale fuel cell systems typically employ vertical-series stack configurations in combination with bulky peripheral devices to regulate gas flows, pressures, stack temperature, and other operating variables. These peripherals allow the fuel cell systems to operate at extremely high efficiency with minimum use of the expensive fuel cell membrane and catalyst materials. In contrast, the drive for maximum power density and miniaturization in portable fuel cell devices means that it is desirable to operate them under ambient conditions with a minimum of peripheral components [3].

Since the voltage output of a single fuel cell is at maximum about 1 V, use of fuel cells in portable devices necessitates interconnection of multiple cells to meet application-specific voltage requirements. However, portability concerns require that the packaging of small-scale fuel cell devices be space-efficient and cost-effective. Thus, the vertical series stack configuration used by large fuel cell systems is most likely an inappropriate solution.

The unique requirements of portable fuel cell systems have led to the formulation of several design alternatives to the conventional vertical-series fuel cell stack. These design alternatives include the banded membrane configuration

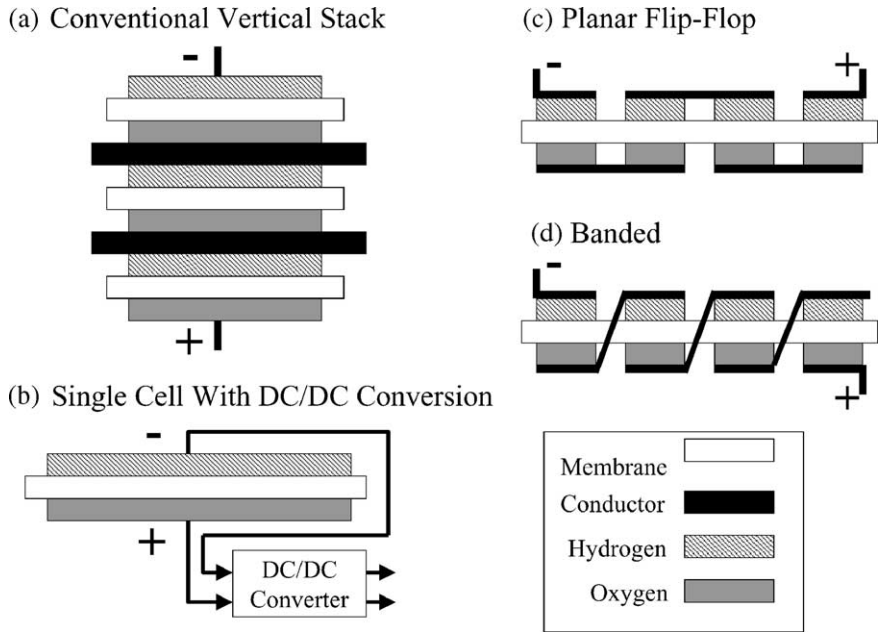

Fig. 2. Stack designs for membrane fuel cells: (a) conventional vertical (bipolar) stack; (b) single cell with dc/dc conversion; (c) planar flip-flop configuration; (d) planar banded configuration.

[4,5], the flip-flop configuration [6], and the single-cell fuel cell with dc–dc converter. These alternative designs are compared along with the conventional vertical-series stack in Fig. 2. A common trait for these design alternatives is that they are planar. For small power applications, these planar designs can have advantages in terms of power density, manufacturability, form factor, and packaging flexibility [7].

Much of the initial work in planar miniature fuel cells focused on the use of silicon-MEMS technologies. Earlier work in our laboratory has demonstrated planar miniature fuel cell prototypes based on silicon technology [8]. Yu et al. [9], Kelley et al. [10], and Min et al. [11] have also reported silicon-based miniature fuel cell devices. Pavio et al. [12] from Motorola have developed planar fuel cell systems using low temperature co-fired ceramic technology. For additional discussion of miniature fuel cell design, the reader is referred to Dyer's [13] article on fuel cells for portable applications and the recent review article of Maynard and Meyers [14].

2. Design and fabrication

An inherent strength of PCB technology is the ability to handle complex planar designs. Additionally, as emphasized earlier, planar design offers significant advantages for portable fuel cell applications. Therefore, the PCB-FC devices we have developed to date incorporate planar fuel cell array design. In particular, the PCB-FC prototypes all employ a modified planar banded configuration (Fig. 2d). As most portable electronic devices operate at voltages in 5–24 V range, a useful fuel cell device must serially interconnect many cells together to provide the necessary voltage requirement. Serially interconnecting a planar array of cells leads to inherently complex in-plane geometries, requiring patterned insulating and conductive regions. However, this design approach actually plays to the strengths of PCB technology, where complexity *within a layer* is preferred to complexity *between layers*. Because the copper metal used in PCB design presents corrosion problems in a fuel cell environment, all copper surfaces were plated with a protective gold layer. Gold plating is standard, widely available PCB specification. This provided the double benefit of eliminating corrosion concerns and also improving the ohmic contact between the membrane electrode assembly (MEA) and the PCB electrodes.

In this section, we will detail several design generations of PCB-FC prototypes. Between design iterations, major differences arise in the cell and array size, gas delivery and flow structure design, and overall power output. Table 1 summarizes the various prototype iterations that are discussed in the paper. The first prototypes used a "sea-serpent" gas delivery design. Several versions of the "sea-serpent" prototype design were implemented with incremental performance improvements. Further PCB-FC development then focused on a new design paradigm, the "micro-stitch" design. Both single cell and modular arrays of the micro-stitch prototype were implemented. General aspects of both the "sea-serpent" and "micro-stitch" prototype designs will be introduced in Sections 2.1 and 2.2. The comparative advantages and disadvantages of the designs are discussed and the iterative improvements of the PCB-FC technology are highlighted.

2.1. "Sea-serpent" fuel cell prototypes

The earliest iterations of PCB-FC prototypes were developed using "sea-serpent" gas routing (to be described

Table 1
Performance summary of the PCB-FC prototypes

Iteration	Type	Dimensions (cm)[a]	Volume (cm^3)	Number of cells	V_{max} (V)	V at P_{max} (V)	P_{max} (absolute; W)	P_{max} (per cell-area; mW/cm^2)	P_{max} (volumetric; mW/cm^3)
1	Sea-serpent bonded	9.7 × 9.7 × 0.4	37.6	64	Negligible performance metrics				
2	Sea-serpent bonded	9.7 × 9.7 × 0.4	37.6	16	12.9	5.5	0.1	6.25	2.7
3	Sea-serpent bonded	9.2 × 10.2 × 0.5	46.9	16	14.3	6.4	1.4	87.5	30
	Sea-serpent clamped	9.2 × 10.2 × 0.5	46.9	16	14.8	6.3	2.5	156	53
4	Micro-stitch bonded	3.9 × 3 × 0.3	3.51	1	0.94	0.45	1.1	540	313
	Micro-stitch clamped	3.9 × 3 × 0.3	3.51	1	0.97	0.40	1.4	700	400
5	Micro-stitch bonded	17 × 27.5 × 1.3	610	12[b]	5.7[b]	3.0[b]	205	380	340

The testing conditions for each prototype are provided in Table 2.
[a] Overall dimensions of the fuel cell device, does not include inlet gas fixtures or the compressed gas supply.
[b] 12 cells; six pairs of cells in series.

shortly). Three generations of the sea-serpent design were tested, each incorporating successive refinements. Fig. 3 (see also Fig. 1a) shows an example of the third iteration "sea-serpent" design. This planar fuel cell design employs 16 series-connected cells to provide between 6 and 12 V at useful current densities. Our discussion of the "sea-serpent" PCB-FC design will be in the context of this prototype, as it was the most successful and refined of the three prototype generations. The generalities of the electrical interconnection, gas delivery structure, and laminate PCB construction apply to all three prototype versions.

2.1.1. Electrical Interconnection

Fig. 3 shows the inner feature boards of the 16-cell "sea-serpent" PCB-FC device. The boards in this photograph provide series electrical interconnection for a planar array of 16 fuel cells. Clearly visible are the gold-coated electrode contacts for the 16 cells in the array and the electrical interconnection pads at the sides of the boards. Series connection requires the bottom electrode of one cell to connect to the top electrode of the next cell. To avoid potential gas leaks across the device, membrane integrity must be maintained. Thus, the series cell interconnections

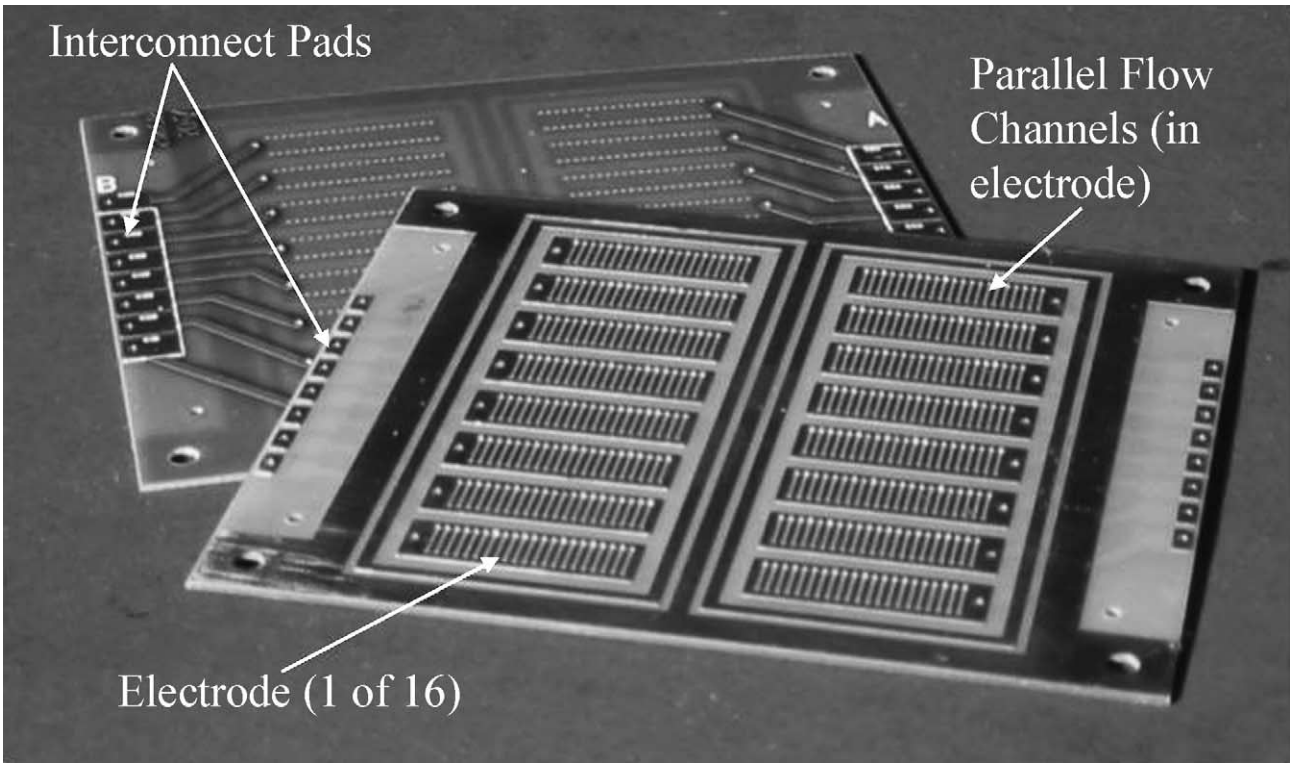

Fig. 3. Inner board detail which shows the array of 16 cell electrode contacts and the 16 perimeter interconnection pads of the third iteration "sea-serpent" PCB-FC prototype.

are made *around* the perimeter of the membrane through externally accessible pads. To separate the cell electrode contacts from the interconnection routing, and to maintain flat topography for pre-preg bonding on the backside of the inner board, the interconnections are routed on an inner layer in the PCB board. Vias connect the inner layer to the front-side electrode contacts and to the interconnection pads on the edges of the board.

2.1.2. Flow routing

Since PCB technology is well suited to handle complex electrical interconnection requirements but is less well developed to handle complex fluid delivery situations, a design was selected that simplified flow routing while minimizing the danger of leaks. This design crucially depended on the ability to create leak proof cavities in a PCB stack using "no-flow" pre-preg bonding (Isola FR406). This ability made it possible to separate the flow routing design from the electrode design. Additionally, the geometric integrity of "no-flow" laminate offered the design freedom to combine void spaces and structural components with a high level of detail by Dean et al. [15].

Reactant distribution plays a vital role in determining the performance of fuel cells. Flow routing must be designed with multiple criteria including minimal pressure loss, uniform reactant distribution, and water removal [16]. The flow geometry for the sea-serpent design was chosen to address the demands of the multiple criteria for flow routing using PCB laminate technology manufacturing processes in the fuel cell prototype. Visible in Fig. 3 are the sea-serpent design's parallel micro-flow channels, each 500 μm wide, which were etched in the copper layer (and later plated with gold for corrosion resistance) in contact with the membrane's carbon cloth electrodes. The narrow channels promote well-controlled positive flow displacement to continually replenish new reactant and to remove water from the product side. Large interdigitated channels in the layer below supply the gasses flowing in the micro-channels. This multi-layer, multi-scale flow distribution approach provides low-resistance, uniform gas distribution. The interdigitated arrangement assures that each cell encounters the same pressure difference and velocity profile between inlet and outlet. Reactant gas streams are forced from an interdigitated entry channel, down into the micro-flow channels parallel to the MEA, and then back up into an interdigitated exit channel, in a "sea-serpent" like flow pattern, thus giving the PCB-FC prototype its name. Appropriately, the micro-channels are patterned by photolithography and etching, while the macro-channel sub-layer is machined by direct milling. In the layers between these channels, bonding is accomplished via "no-flow" pre-preg.

2.1.3. Laminate construction

A schematic of the electrode structure is shown in Fig. 4 (middle). Clearly visible are the gold-plated copper cutouts for micro-parallel gas flow and the through holes for gas delivery from the underlying macro-flow structure. The micro-flow channel height is given by the thickness of the copper layer on the top board. Gold-coated copper surrounds each electrode flow channel and thus together with the membrane prevents any fuel leak outside the channel. During the fuel cell operation, water is generated as a byproduct. This cell design prevents water trapping between neighboring cells that might otherwise lead to short currents.

The half-cell consists of three FR4 boards bonded together with no-flow pre-preg inserts. The inner board contains the electrodes, micro-parallel flow channels, and holes in each channel for reactant entry and exit. The middle board and the backplane create the interdigitated macro-flow routing layer. An exploded view showing the multiple layers that compose the laminate PCB fuel cell prototype is shown in Fig. 5.

2.2. "Micro-stitch" fuel cell prototypes

Later versions of the PCB-FC were developed using a new flow-routing scheme, which we will call the "micro-stitch" design. The "micro-stitch" scheme is similar to an interdigitated flow structure delivery system, forcing gas through the fuel cell MEA from a set of inlet ports to a set of outlet ports. It will be described in detail shortly. As with the "sea-serpent" design, several iterations of the micro-stitch were developed. First, single cell micro-stitch devices were constructed to verify the principle of the design. Then the design was extended into multiple-cell planar array configurations.

2.2.1. Flow geometry

The micro-stitch design consists of a grid of alternating gas inlet and outlet ports fed by channels such that the gas enters and exits normal to the membrane electrode assembly (Fig. 6). In this configuration, each gas inlet is surrounded by four gas exits, facilitating a widely spread flow that penetrates deep into the carbon cloth. Patterning drilled holes in PCB, such as those functioning as gas ports in the micro-stitch design is part of the standard PCB fabrication process.

2.2.2. Small-scale prototyping

A series of prototype cells utilizing the micro-stitch design were manufactured. With an active area of only 2 cm^2, these cells were inexpensive and easy to produce. A 2 cm^2 micro-stitch cell consists of two small squares of PCB, one for each gas, with the micro-stitch hole pattern drilled in the center of each. The cell takes advantage of multi-layer PCB design by routing the electrodes from the active area surface to the interior of the PCB, using the gas ports as electrical vias. The internal copper routing extends to the edge of the PCB where another via brings the electrical connection to a gold-plated tab on the surface for improved access as pictured in part (b) of Fig. 1. Interdigitated channels with a width equal to the hole size of 15 thousandths of an inch

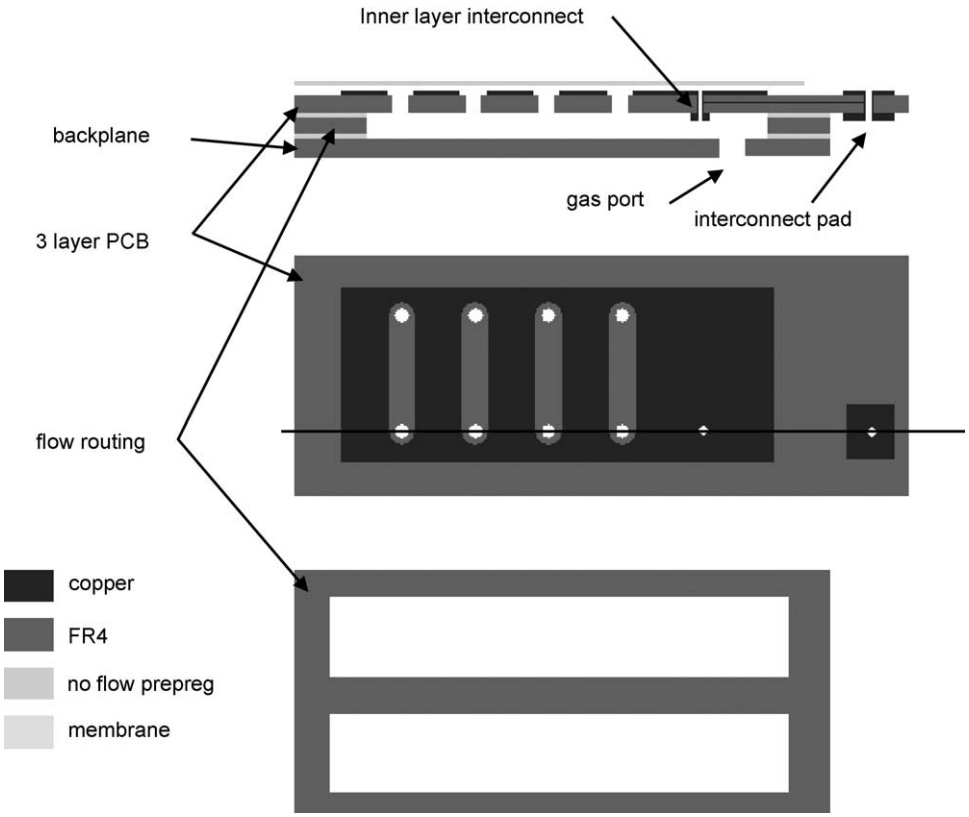

Fig. 4. Simplified schematic illustration of a one-half of a single cell in the third iteration "sea-serpent" PCB array. The inner board provides the electrode contact to the MEA and the micro-parallel fluid delivery of reactants. The backing layers provide the macroscopic interdigitated flow routing and gas porting. Interconnect pads on the perimeter of the device (external to the MEA) provide series connection between cells.

and an aspect ratio of unity were machined on the backside (non-electrode side) of the feature PCBs to connect columns of gas ports. A small manifold area was also machined to feed gas to the channels.

2.2.3. Micro-stitch high power array

An additional goal of the micro-stitch development was to explore the upper end of our PCB-FC power generating ability. One of the benefits of the micro-stitch flow-routing design is that it inherently scales well over a wide range of cell sizes. Unlike channel-based flow-routing paradigms, where gas depletion down the length of the channel can become a problem for longer channels, the flow situation at the MEA surface is uniform over the entire surface of a micro-stitch cell. As long as the pressure drop in the structures feeding each micro-stitch port can be minimized, uniform operation

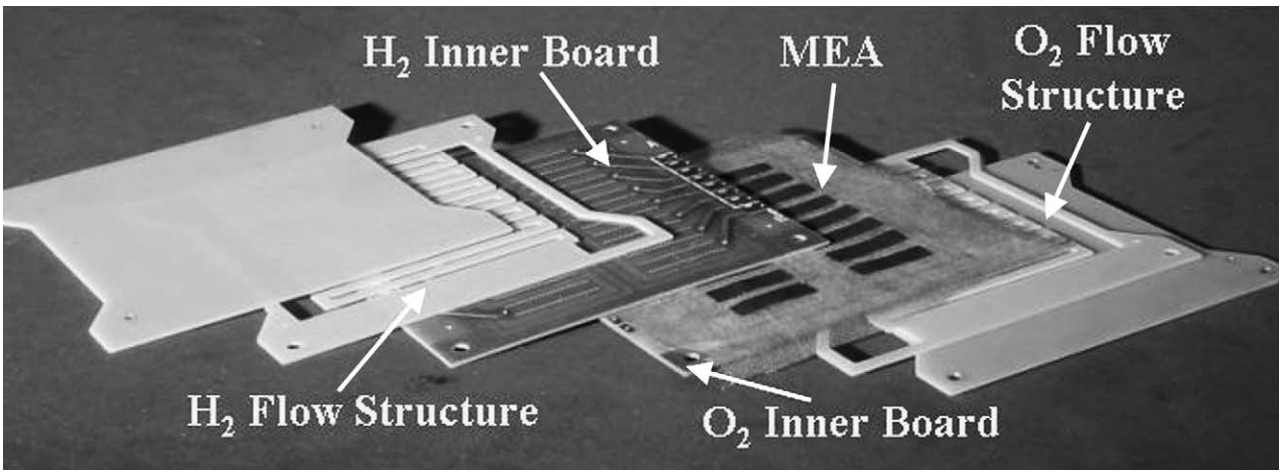

Fig. 5. Exploded detail of the laminates in the third iteration "sea-serpent" PCB-FC. Pre-preg layers are not shown.

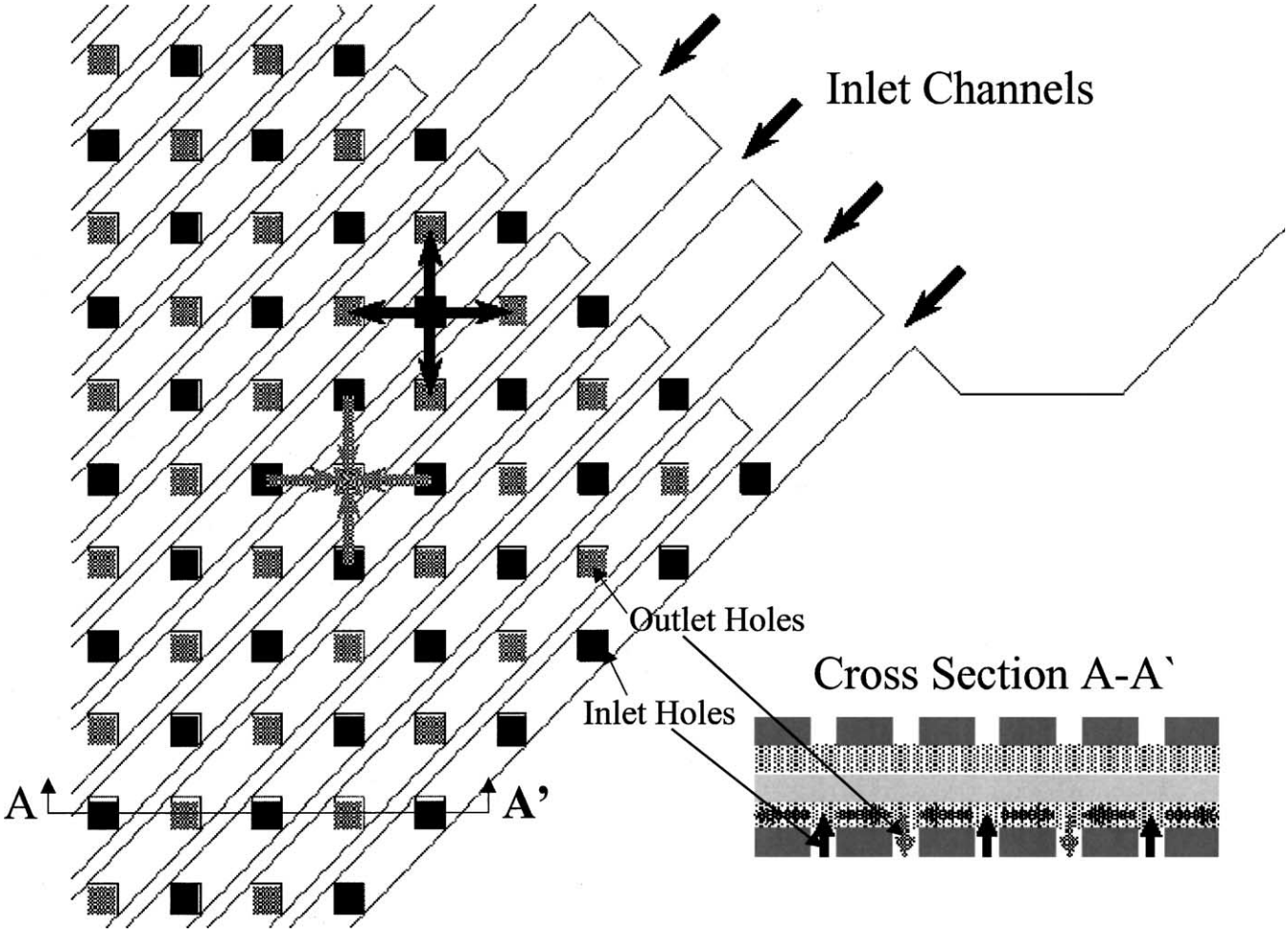

Fig. 6. Schematic illustration of the micro-stitch flow design showing a top and side view of the gas ports and their associated flow directions.

across all ports is easily achieved. In addition to the need for uniform gas distribution within each cell, for high power arrays there is also the need to ensure uniform gas distribution between cells. To achieve both these goals, a novel macro-scale manifold structure supplying the micro-scale flow structure was developed for the micro-stitch high power array. An exploded view of the manifold is presented in Fig. 7, showing how gas is routed between layers to each of the six cells on one MEA.

For the micro-stitch high power array as depicted in Fig. 1c, our design combined two MEAs per board, creating a "double board" configuration. Merits of the double board include the ability to share gases between membranes, space savings due to the gas sharing, and the resulting increase in volumetric power density. Both membranes still employ the planar banded arrangement described earlier, however, the double board allows for better packing density when planar space is constrained. Each outer layer of the double board was laser cut or machined as appropriate, while the electrodes of the inner micro-stitch layer were patterned with photolithography. For assembly, all layers of the double board were pre-preg bonded in a high pressure, low temperature process with Isola A11.

3. Experimental

A summary of the experimental conditions is reported in Table 2. Most prototype designs were first tested with silicon rubber gasket seals under mechanical compression prior to laminate bonding. Testing with mechanically clamped and gasketed protptypes allowed easy assembly, disassembly, re-use, and replacement of the component parts. After prototype functionality was verified, the parts were permanently sealed and laminated together using no-flow pre-preg laminate bonding. Without exception, the mechanically clamped assemblies in each iteration performed better than the laminate bonded free-standing assemblies for that same iteration.

All fuel cell measurements were conducted at room temperature using dry hydrogen and dry oxygen gas. Flow rates were regulated to 2× stochiometric or less using indepen-

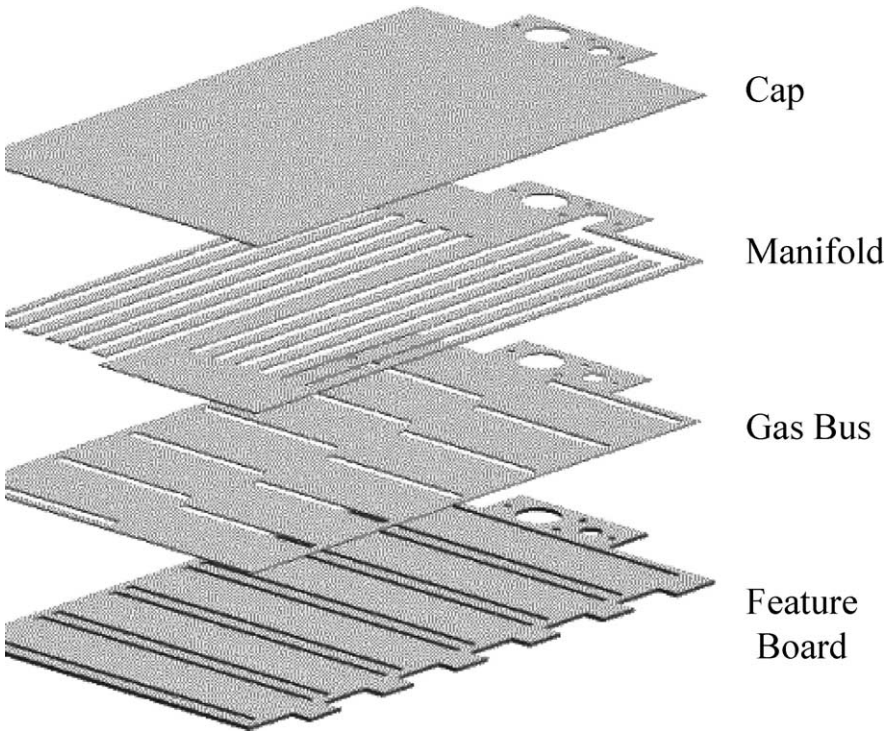

Fig. 7. Exploded detail of the gas manifold structure supplying each cell of the micro-stitch high power array. Pre-preg layers are not shown.

dent mass flow controllers (Alicat Scientific) for H_2 and O_2 (actual flow rates for each test are reported in Table 2). Pressure drops within the fuel cell devices were monitored via inlet pressure gauges and are also reported in Table 2. (The fuel cell outlets vented directly to atmosphere so the pressure at the inlet of the fuel cell (in psig) must also represent the pressure drop within the fuel cell.) Although the tests were nominally conducted at room temperature, significant self-heating (particularly for the larger fuel cells) was observed. Thermocouples attached to the outside surface of the PCB fuel cell devices during the later fuel cell tests generally read between 30 and 50 °C during operation (see Table 2).

Table 2
Summary of experimental conditions for the PCB-FC prototypes

Iteration	Type	Preconditioning	O_2 flow rate at maximum current (sccm)	H_2 flow rate at maximum current (sccm)	Pressure drop at maximum flow rate (PSI)	External cell temperature at 0.6 V (measured; T_0; °C)	Internal cell temperature at 0.6 V (estimated)	Average test duration (min)
1	Sea-serpent bonded	NA	5	10	<0.1	NA	NA	NA
2	Sea-serpent bonded	Cell re-hydration[a], then 30 min at the rate of 0.4 V	5	10	<0.1	NA	$T_0 + 1$ °C	30
3	Sea-serpent bonded	Cell re-hydration[a], then 30 min at the rate of 0.4 V	60	120	<0.1	NA	$T_0 + 8$ °C	30
	Sea-serpent clamped	Cell re-hydration[a], then 30 min at the rate of 0.4 V	80	160	<0.1	NA	$T_0 + 11$ °C	30
4	Micro-stitch bonded	Cell re-hydration[a], then 10 min at the rate of 0.5 A	20	40	0.25	41	60.8 °C	90
	Micro-stitch clamped	Cell re-hydration[a], then 10 min at the rate of 0.5 A	23	40	0.25	33.8	60.3 °C	90
5	Micro-stitch bonded	Cell-by-cell re-hydration[a], then 5 min at the rate of 15 A	3500	7000	2.0	46	104.8 °C	30[b]

The performance metrics for each prototype are provided in Table 1.

[a]Cell re-hydration involved subjecting the fuel cell to a curent load, thereby, generating liquid water which hydrated the cell. The current load on the cell was steadily increased with time until time stable performance was achieved (i.e. stable voltage output over a 5 min period). This re-hydration period typically took 30–60 min for the small cells (iterations 1–4) but only about 5 min per cell for the large area cells (iteration 5). See Fig. 8.

[b]Overheating leads to performance instability above 40 A.

Temperature measurements inside the fuel cells at the MEA were not taken, but can be estimated from the temperatures measured at the exterior of the PCB devices and the materials properties of FR4.

Assuming steady-state heat flow, Fourier's first law can be used to estimate the internal temperature of the PCB fuel cell devices (Eq. (1)):

$$Q = -\lambda \frac{T_0 - T_i}{\delta} \quad (1)$$

where T_i is the internal temperature, T_0 the external temperature (measured on the external surface of the fuel cell, thus T_0 may still be greater than the ambient room temperature), δ the thickness of the FR4, λ the thermal conductivity of FR4 ($\lambda_{FR4} = 1.7 \times 10^{-3}$ W/cm K), and Q the heat flux generated by the fuel cell. Q is assumed to be the steady-state heat output of the fuel cell at 0.6 V, it can be obtained from the IV curve (Eq. (2)).

$$Q = \tfrac{1}{2}(1.2 - 0.6)J|_{0.6\,V} \quad (2)$$

Where J (A/cm^2) is the current density of the fuel cell. The heat generated is assumed to be distributed uniformly over the area of the cell and the factor of 1/2 arises due to the assumption that half of the heat is conducted away in each direction.

This simple calculation neglects any heat that is removed by the gasses flowing within the fuel cell, and hence likely *overestimates* the true internal temperature. The results of these estimations are also summarized in Table 2. Additional discussion of the self-heating effect and its impact on cell performance is planned for a future contribution.

Commercial MEAs were obtained from BCS Technologies Inc. (Byran, TX). The MEAs were constructed with standard hot-pressed carbon cloth electrodes, Pt/C catalyst ink (2 mg/cm^2 Pt) and Nafion 112 membrane. The MEAs employed a self-humidification technology, (BCS Technologies) the details of which cannot be provided. Low power measurements (<2 W, <750 mA) were acquired via a Gamry PC4/750 potentiostat system linked to a PC. High power measurements (>2 W, >750 mA) were obtained with an HP 6050A electronic load mainframe with HP-60504B load module.

A preconditioning period was utilized prior to measurement. Also, the lamination procedure employed during device fabrication severely dried the Nafion membrane, making it necessary to re-hydrate the MEA. Re-hydration and preconditioning procedures are documented in Table 2. An important distinction is made regarding re-hydration versus preconditioning, re-hydration was performed only once on each device after the hot-lamination assembly step dried out the MEA, preconditioning was a standard pre-test cycle applied before every fuel cell test run. An example of the first 20 min of a re-hydration procedure on a 2 cm^2 cell is documented in Fig. 8. Performance generally increased gradually even after the preconditioning period, suggesting full warm-up of the MEA takes some time. As an example, Fig. 9 relates a series of voltage versus current density (IV) measurements made during testing of a 2 cm^2 pre-preg bonded micro-stitch PCB-FC. The three IV curves were taken right after preconditioning, 90 min into the test, and 135 min into the test respectively. During a 180 min test of a clamped 2 cm^2 micro-stitch PCB-FC, maximum power density increased from

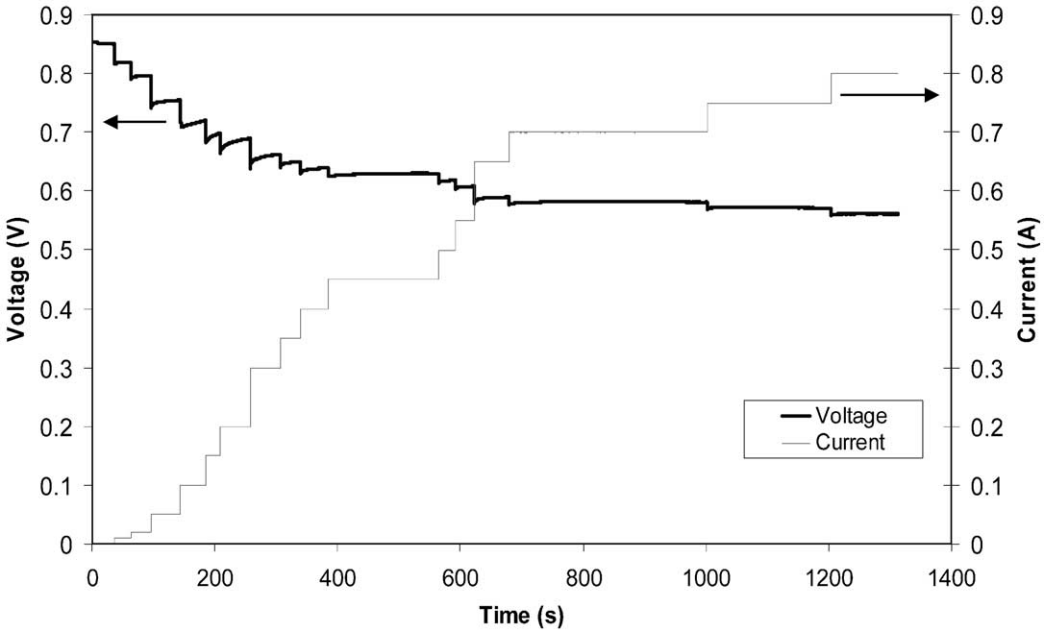

Fig. 8. Re-hydration cycle for a 2 cm^2 PCB-FC. Voltage and current traces are recorded vs. time under the standard experimental conditions documented in Table 2. The current load on the cell was steadily increased until time stable performance was achieved. The first 20 min of the re-hydration cycle are shown.

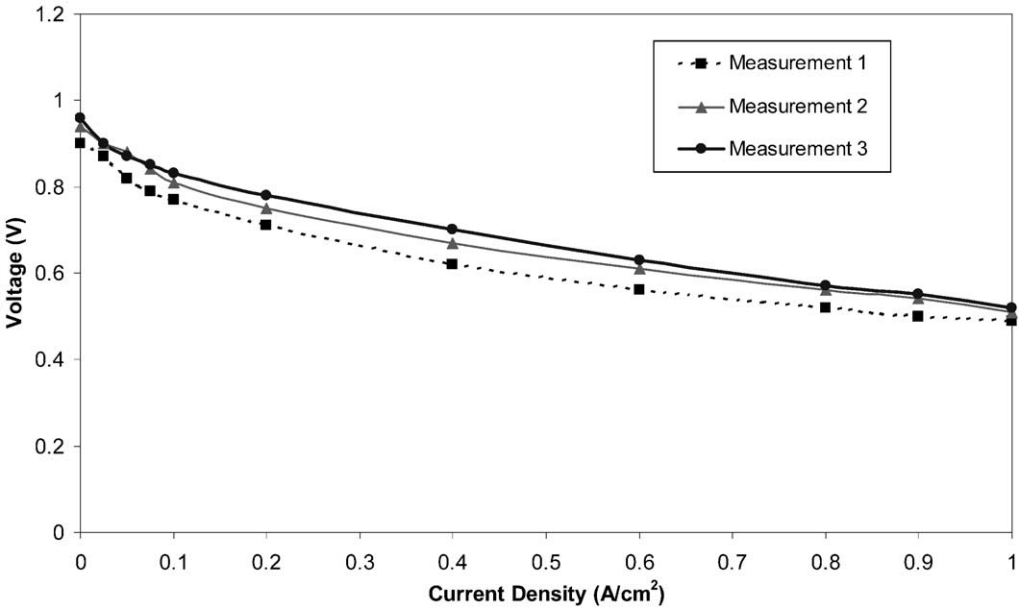

Fig. 9. Voltage vs. current density at various time intervals during a 135 min test of a 2 cm^2 pre-preg bonded micro-stitch PCBFC. Measurement 1 (■) was taken immediately after preconditioning. Measurement 2 (▲) was taken 90 min into the test. Measurement 3 (●) was taken 135 min into the test. Testing conditions are provided in Table 2.

704 to 713 mW/cm^2. During a 45 min potentiostatic run of a 2 cm^2 pre-preg bonded micro-stitch PCB-FC at 0.516 V, current density decreased slightly from 0.85 to 0.84 A/cm^2. Stability was an issue for the fifth iteration micro-stitch array due to suspected overheating at currents larger than 40 A. Long-term operation tests were not conducted.

4. Performance results

Figs. 10 and 11 summarize the typical IV and power density results obtained for the second to fifth prototype iterations. These results have been normalized to per-cell, per-unit area figures in order to fairly compare the various prototype generations. Several general features should be noted. First, as mentioned above, the clamped assemblies perform better than their laminate bonded counterparts. The performance degradation in the laminate bonded assemblies may be attributed to several possible causes.

(1) The heat cycle during the lamination process (160 °C) may irreversibly harm membrane conductivity or cause damage to the catalyst layer.
(2) Lamination bonding may result in decreased ohmic contact between PCB electrodes and MEA compared to that achieved with direct mechanical compression.
(3) Excessive force during bonding can pinch off flow-channels and other gas routing features, reducing gas access to portions of the MEA.

Secondly, note the dramatic improvement over successive prototype iterations. Rapid performance improvement was possible due to the mature nature of PCB technology and the availability of quick PCB prototype turnarounds. The most significant design improvements:

(1) Laminate bonding optimization.
(2) Improved flow structure design.
(3) Area-utilization improvements.

The absolute performance of the fifth iteration prototype is shown separately in Fig. 12. The fifth iteration prototype design was motivated from a desire to demonstrate the high power capability of the PCB-FC platform. Fig. 12 thus shows the absolute performance behavior of this design iteration rather than relative performance. As can be seen from the figure, the fifth iteration micro-stitch array bonded delivers over 200 W. This 12-cell board was tested with six pairs of cells in series, resulting in V_{max} of 5.7 V. (Pairing cells allowed us to deliver higher currents that were necessary for a particular application, it also demonstrates the ease of voltage configurability for these planar arrays.) A photograph of this prototype was shown in Fig. 1c. Note from Table 1 and Figs. 10 and 11 that the relative performance (in terms of power density, current density) of this final prototype is somewhat lower than that of the single cell fourth iteration prototype. No attempt was made to make further refinement in design for this fifth iteration prototype compared to the previous iteration. The decreased performance may be explained by increased reactant distribution, water flooding, and overheating problems encountered by this large array prototype compared to the small single cell prototype.

Any useful miniature fuel cell device will likely run on air rather than pure O_2. In this study, pure oxygen from a

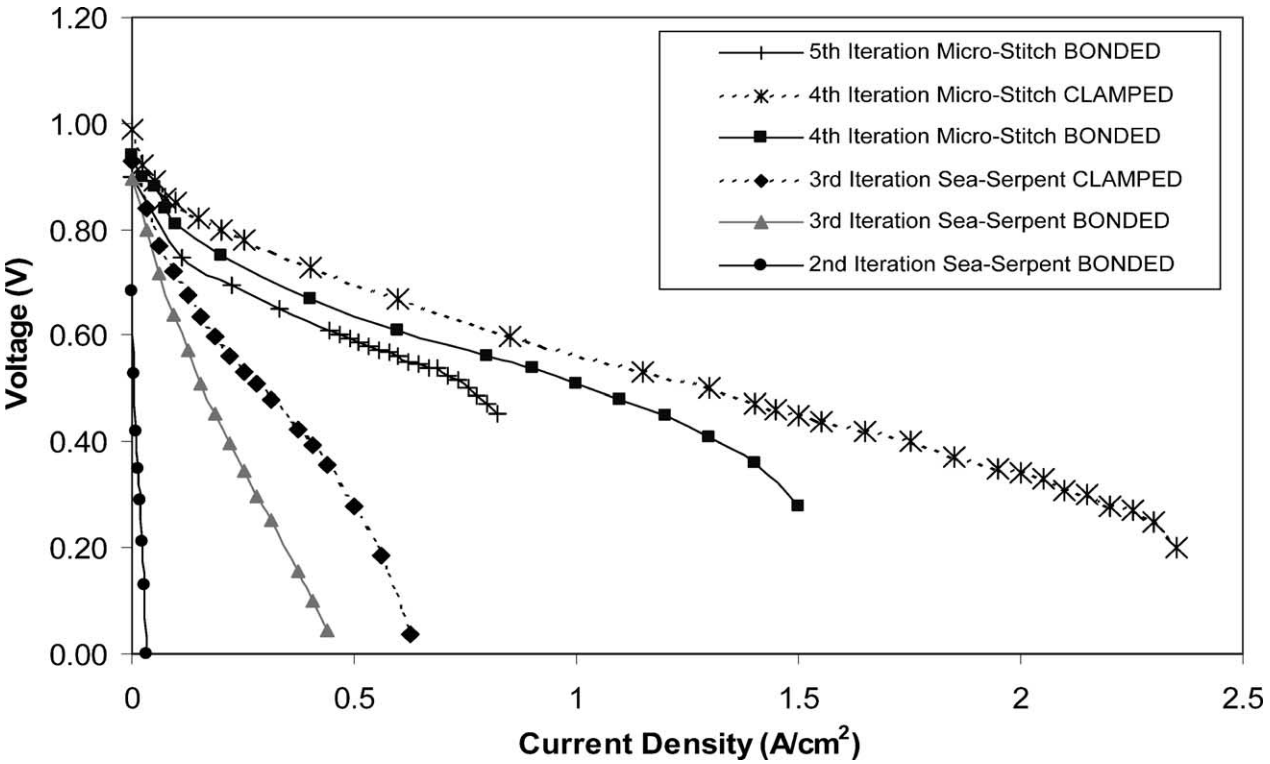

Fig. 10. Relative voltage vs. current density performance comparison of the second to fifth prototype generations normalized to a per-cell, per unit area basis. Testing conditions are provided in Table 2.

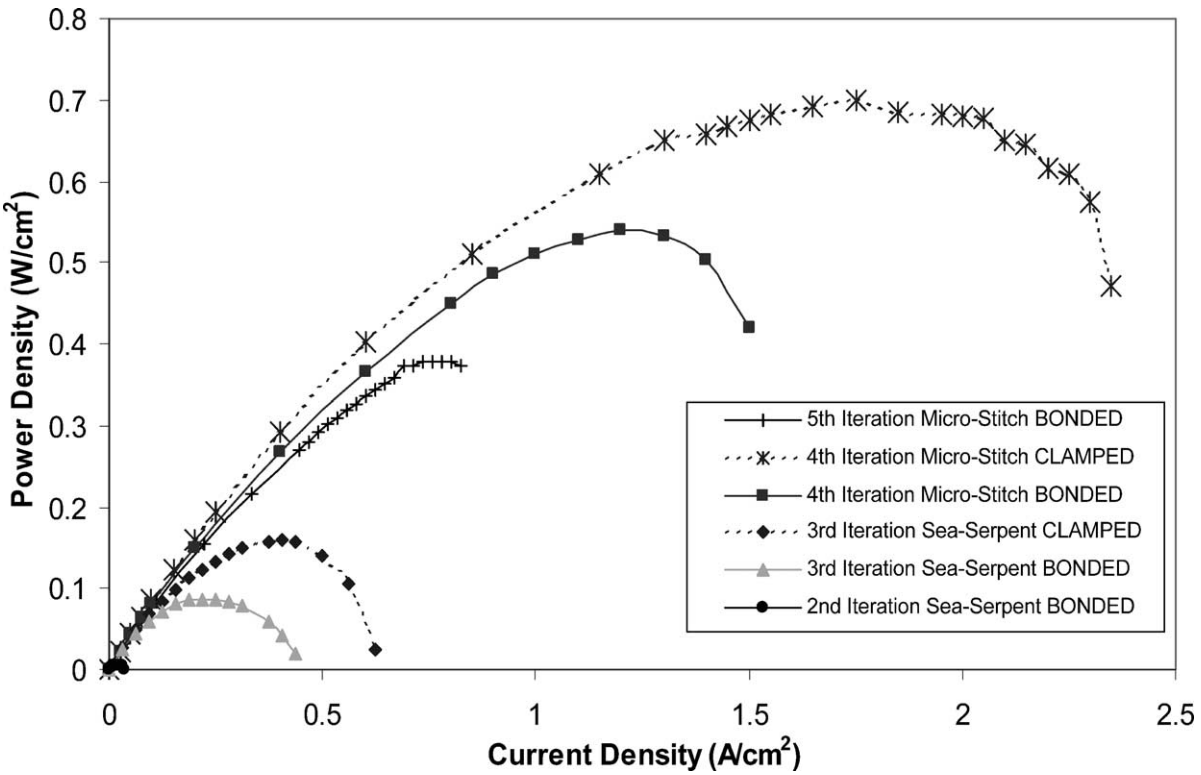

Fig. 11. Relative power density comparison of the second to fifth prototype generations. Power performance has been normalized to a per-cell, per unit area basis. Testing conditions are provided in Table 2.

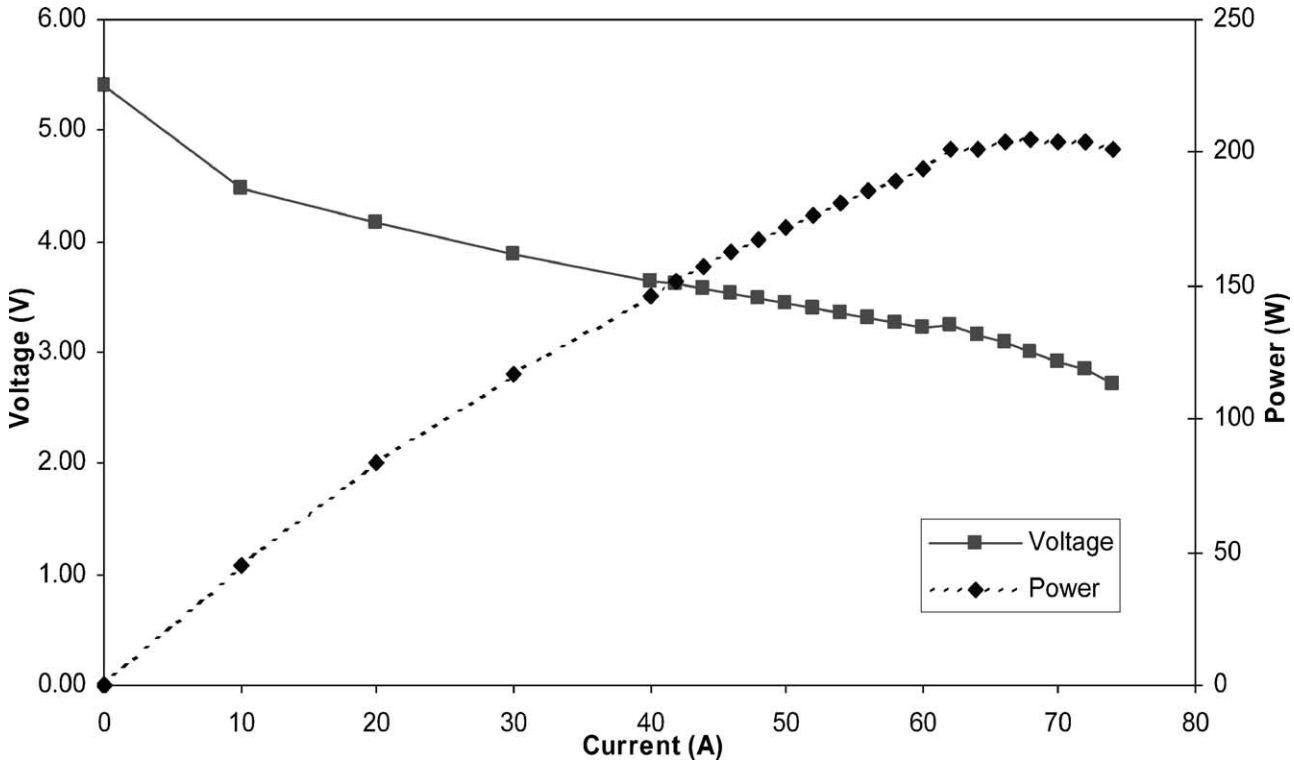

Fig. 12. Total voltage and power performance of the fifth iteration micro-stitch array bonded PCB-FC. To demonstrate the flexible-configuration ability of the design, the 12 cells were linked in pairs, creating a device with a maximum 5.7 V OCV, but doubling the current output. Testing conditions provided in Table 2.

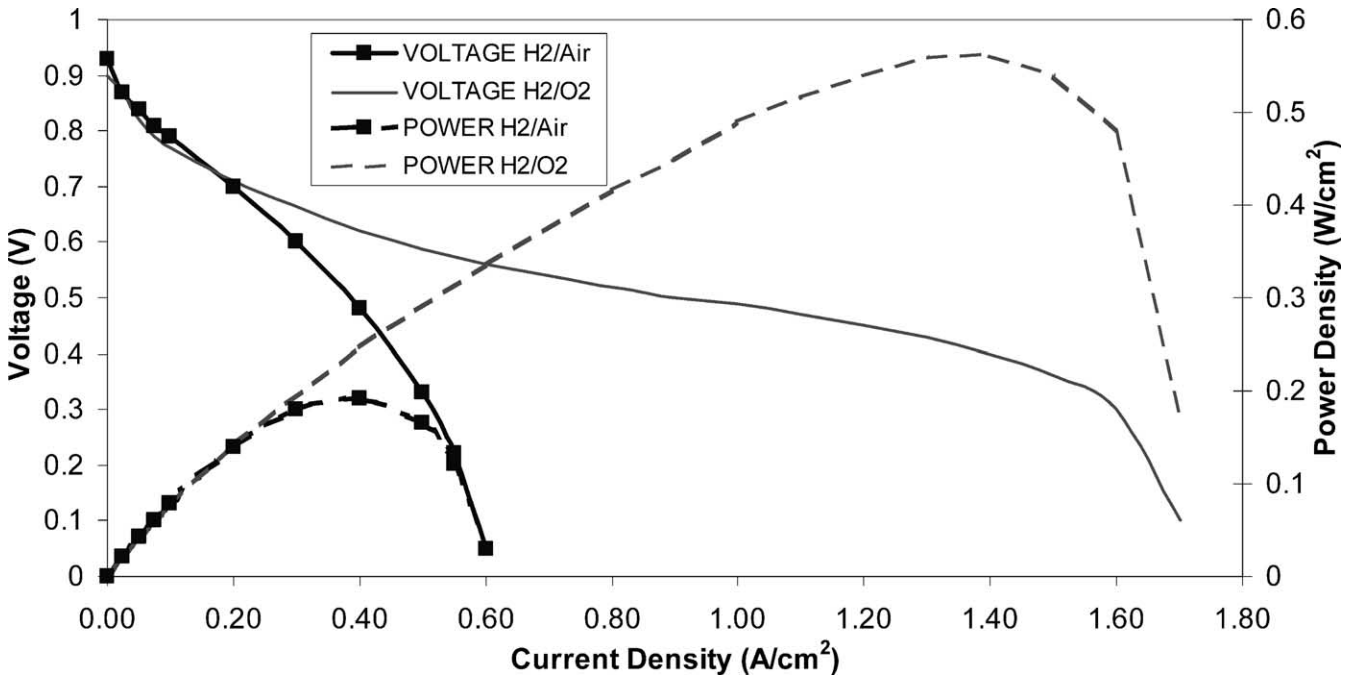

Fig. 13. Comparison of a fourth iteration bonded 2 cm^2 micro-stitch PCB-FC prototype running on pure oxygen vs. air (■). The pure oxygen data was obtained using the same testing conditions as previously noted in Table 2. For the H_2/air test, flow rates at max current were 30/60 sccm, respectively; pressure drop through the cell at max air-flow was 2 psi.

compressed gas cylinder was used for all tests, eliminating the need for valves, pumps, or a passive air-breathing design. Performance on air has been investigated for a bonded 2 cm^2 micro-stitch prototype, the results of which are compared in Fig. 13 to the previous data on pure oxygen. Air was supplied from a compressed gas cylinder. H_2/air flow rates at max current were 30/60 sccm, respectively, pressure drop through the cell at max air-flow was 2 psi, cell heating was similar to the results shown in Table 2 for previous 2 cm^2 micro-stitch tests, test duration was 1 h. The same preconditioning cycle was used as for the H_2/O_2 micro-stitch test, but with air. As is shown in the figure, maximum power density is reduced by approximately a factor of three versus pure oxygen.

5. Conclusions

For a synopsis of our major prototype results, the reader is referred to Table 1, which summarizes the absolute performance specifications of the various prototype designs presented in the paper.

In the introduction, many of the potential benefits of the PCB-FC platform were summarized. Over the course of prototype development, these advantages have proven to be enormously helpful in the rapid advance of the PCB-FC technology. Less anticipated, however, were advantages related to scaling flexibility. The ability to easily scale device voltage has proven to be a major benefit for the PCB planar-array design. We have been able to configure voltage outputs ranging from 1 V single cell designs to 16 V multi-cell designs with little additional complication from an assembly perspective. This has also proven to be a major prototyping advantage. Another highly advantageous aspect of PCB-FC design has been the ability to scale over a wide power range. While we have demonstrated PCB-FC power sources ranging from less than one watt to several hundred watts, we estimate the upper end of PCB-FC application at around 1 kW. Above this level, the increasing demand for more robust current collectors and improved cooling suggest the adoption of alternate materials and stack design strategies.

A forced air-design with an external pump does not appear attractive, as the parasitic power losses from the pump are estimated at 20–25% of the total power output. Passive-air breathing designs using PCB are intriguing. In fact, a passive-air breathing design suits the PCB planar-array paradigm nicely and would be considerably less complex, due to the elimination of the manifold layers from the air side. Demonstration of a passive air-breathing array is a future goal.

Continued power density improvements can also be expected. Possible avenues of development include the use of thinner PCB boards (possibly even flex-circuit technology—flexible fuel cells), more efficient gas routing, improved bonding and sealing, and intelligent cell array design aimed at reducing perimeter to area ratios. Plans for further prototype iterations using these approaches to increase volumetric power density are currently underway. Special care must be taken in planar designs to avoid incurring significant lateral conduction losses between cells when attempting to increase power density by reducing cell-to-cell spacing [17].

In addition to simple power density improvements, it is interesting to consider further possible synergies in the combination of PCB and fuel cells. Because the fuel cell devices are built on PCB substrates, it is attractive to consider the addition of electronic components such as internal diagnostics (thermocouples, sensors), on board control circuitry, or even active electronic components such as actuators, valves, and pumps to regulate fuel supply. The current voltage configurability of a PCB fuel cell could be automated with the integration of programmable electronic switches. Voltage/current outputs of a fuel cell array could then be configured and adjusted on the fly-essentially making for an adaptable power supply. An ultimate goal is the full integration of fuel reservoir, processing, and supply. All the necessary elements for an on-board methanol/borohydride reservoir, micro-fluidic catalytic reformer, and fuel regulation/delivery system currently exist, although it is admittedly a significant engineering challenge to couple them together in an integrated system.

Acknowledgements

The authors would like to acknowledge financial support of this work by Honda R&D Co., Ltd. This material is based upon work supported under a Stanford Graduate Fellowship, and from support by the Stanford Summer Research College. Han-Kuang Chu, Kai Fan, Rojana Pornprasertsuk, and Won Hyoung Ryu deserve special thanks for obtaining the time-resolved data documenting our typical re-hydration cycle procedures.

References

[1] R. O'Hayre, S.W. Cha, T. Fabian, S.J. Lee, Y. Saito, F.B. Prinz, Development of a miniature fuel cell array with printed circuit technology, in: Proceedings of the Presentation at the 2002 International Manufacturing and Packaging Society MEMS 2002 Workshop, 8 September 2002.
[2] U.S. Provisional Patent, Application 60/379, 524 filed May 9, 2002. U.S. Full Patent Application 10/435 filed May 9, 2003.
[3] A. Heinzel, C. Hebling, M. Muller, M. Zedda, C. Muller, J. Power Sources 105 (2002) 250.
[4] A. Heinzel, R. Nolte, K. Ledjeff-Hey, M. Zedda, Electrochim. Acta 43 (1998) 3817.
[5] K. Ledjeff, R. Nolte, DE 4329,819 EP 0711461, DE 4443,939, DE 4443,945, DE 195,02,391.
[6] S.J. Lee, S.W. Cha, Y.C. Liu, R. O'Hayre, F.B. Prinz, in: K. Zaghib, S. Surampudi (Eds.), Proceeding of the Electrochemical Society Series on the Micro Power Sources, PV 2000–2003, Pennington, NJ, 2000.
[7] R. Nolte, A Kolbe, K. Ledjeff-Hey, in: Proceedings of the 37th Power Sources Conference, 17–20 June 1996, pp. 77–80.
[8] S.J. Lee, A. Chang-Chien, S.W. Cha, R. O'Hayre, Y.I. Park, Y. Saito, F.B. Prinz, J. Power Sources 112 (2002) 410.
[9] J.R. Yu, P. Cheng, Z.Q. Ma, Electrochem. Acta 48 (2003) 1537.

[10] S.C. Kelley, G.A. Deluga, W.H. Smyrl, Electrochem. Solid State Lett. 3 (2000) 407.
[11] K.B. Min, S. Tanaka, M. Esashi, Electrochemistry 70 (2002) 924.
[12] J. Pavio, J. Bostaph, A. Fisher, J. Hallmark, B.J. Mylan, C. Xie, Adv. Microelectron. 29 (2002) 8.
[13] C.K. Dyer, J. Power Sources 106 (2002) 31.
[14] H.L. Maynard, J.P. Meyers, J. Vac. Sci. Technol. B 20 (2002) 1287.
[15] R. Dean, A. Matras, L. Thomas, H. Garrison, N. Schutz, K. MacAllister, S. Tully, A Laminate Based MEMS Accelerometer, in: Proceedings of the Third Advanced Technology Workshop on Packaging of MEMS and Related Micro Integrated Nano Systems, IMAPS, 8–10 November 2001.
[16] A. Heinzel, C. Hebling, M. Muller, M. Zedda, C. Muller, J. Power Sources 105 (2002) 250.
[17] R. O'Hayre, T. Fabian, S.J. Lee, F.B. Prinz, J. Electrochem. Soc. 150 (2003) A430.